Journal of ELECTRONIC MATERIALS, Vol. 45, No. 1, 2016
DOI: 10.1007/s11664-015-4143-4
© 2015 The Minerals, Metals & Materials Society

Optimization of Thermoelectric Performance of Anisotropic $Ag_xSn_{1-x}Se$ Compounds

HUAQIAN LENG,[1,2,3] MIN ZHOU,[1,4] JIE ZHAO,[1,2,5] YEMAO HAN,[1,2,6] and LAIFENG LI[1,7]

1.—State Key Laboratory of Technologies in Space Cryogenic Propellants, Technical Institute of Physics and Chemistry, Chinese Academy of Sciences, Beijing, China. 2.—University of Chinese Academy of Sciences, Beijing, China. 3.—e-mail: lenghuaqian@mail.ipc.ac.cn. 4.—e-mail: mzhou@mail.ipc.ac.cn. 5.—e-mail: zhaojie12@mail.ipc.ac.cn. 6.—e-mail: hanym@mail.ipc.ac.cn. 7.—e-mail: laifengli@mail.ipc.ac.cn

SnSe is a promising thermoelectric material due to its ultralow thermal conductivity. However, stoichiometric SnSe compounds exhibit very low intrinsic defect concentration (3×10^{17} cm^{-3}) and poor electrical transport properties, limiting the thermoelectric performance. In the present work, we investigated the effect of Ag dopant on the thermoelectric properties of SnSe. The results demonstrate that all the $Ag_xSn_{1-x}Se$ compounds exhibited anisotropic thermoelectric properties. The carrier concentration in the $Ag_xSn_{1-x}Se$ compounds greatly increased with increase of the Ag content, saturating at 1.9×10^{19} cm^{-3} for $Ag_{0.01}Sn_{0.99}Se$ at room temperature. We found that a maximum zT value of 0.74 was obtained for $Ag_{0.01}Sn_{0.99}Se$ perpendicular to the pressing direction at 823 K, being 23% higher than that of undoped SnSe (zT = 0.6).

Key words: Thermoelectric performance, SnSe, anisotropy, spark plasma sintering

INTRODUCTION

Thermoelectric materials have attracted considerable attention during recent decades due to their potential application in direct conversion of waste heat into electricity. The thermoelectric performance of materials can be quantified by the dimensionless figure of merit $zT = S^2\sigma T/\kappa$, where S, σ, κ, and T are the Seebeck coefficient, electrical conductivity, thermal conductivity, and absolute temperature, respectively.[1] Accordingly, good thermoelectric materials should possess relatively high power factor ($S^2\sigma$) but low thermal conductivity (κ). Continuous efforts have been made to improve the electrical transport properties[2–4] and decrease the thermal conductivity.[5–8] It is well known that lead chalcogenide IV–VI compounds, such as PbTe,[9,10] PbSe,[11,12] and PbS,[13,14] are excellent thermoelectric materials. However, Pb is toxic to humans and the environment. Moreover, the content of Te in the Earth's crust is very low. Those two factors limit the application of lead chalcogenides.

SnSe is a IV–VI compound with nontoxic and environmentally friendly characteristics. Different from lead chalcogenides, SnSe crystal at low temperature is made up of tightly bound double layers of Sn and Se atoms stacked along the c-axis. Each atom has three strongly bonded neighbors within its own layer and three more distant, weakly bonded neighbors, one of which lies in an adjacent layer.[15] The bonding between layers is of weak, van der Waals type. The thermoelectric properties of SnSe crystal with high zT value of 2.6 along the b-axis at 950 K were reported by Zhao et al.[16] However, the specific structure, i.e., van der Waals bonding, results in weak mechanical properties for single-crystal SnSe. It is expected that optimized polycrystalline SnSe will offer both excellent thermoelectric performance and high mechanical strength.

Recently, the thermoelectric properties of polycrystalline SnSe compounds were reported by Sassi

(Received May 19, 2015; accepted October 9, 2015; published online October 28, 2015)

et al.,[17] displaying significant anisotropy in the transport properties as well as low thermal conductivity. A maximum zT value of 0.5 was obtained. Considering its very high resistivity due to its low intrinsic defect concentration, tuning the carrier concentration and refining the degree of orientation are prospective methods to optimize the electrical transport properties of polycrystalline SnSe. Various candidate dopants (Na, Ag, and Tl) were attempted by Chen and coworkers,[18] but only Na and Ag seemed to be able to be doped and increase the carrier concentration. A saturated carrier concentration of 9×10^{18} cm^{-3} and a peak zT of 0.6 were obtained for Ag-doped polycrystalline SnSe using melting and hot pressing (HP).[18] Nevertheless, the efficiency of Ag doping in SnSe compounds is only around 1%, and the secondary phase $AgSnSe_2$ was observed. Spark plasma sintering (SPS), as a prospective method for fabricating bulk materials, has the advantage of improving the sinterability of poorly sinterable compounds, including the absence of undesired secondary phases.[19] In the SPS sintering process, the powder interfaces are cleaned and activated by a pulsed electric current field, so the powders are densified by strong electric current in short time at low temperature.

In this work, we focused on tuning the carrier concentration and the anisotropic thermoelectric properties of $Ag_xSn_{1-x}Se$ polycrystalline compounds. The thermoelectric properties of $Ag_xSn_{1-x}Se$ were investigated both perpendicular and parallel to the pressing direction. A series of p-type $Ag_xSn_{1-x}Se$ (x = 0.0025 to 0.02) polycrystalline samples were successfully fabricated by melting and SPS methods. The undesired secondary phases were suppressed by the SPS method, and a saturated carrier concentration of 1.9×10^{19} cm^{-3} was obtained for $Ag_{0.01}Sn_{0.99}Se$, which is higher than that obtained by the hot-pressing method. The maximum zT value of 0.74 was observed for $Ag_{0.01}Sn_{0.99}Se$ perpendicular to the pressing direction at 823 K. Parallel to the pressing direction, a maximum zT value of 0.67 was obtained at 823 K.

EXPERIMENTAL PROCEDURES

Weighed elemental tin (Sn, 99.999%), selenium (Se, 99.999%), and silver (Ag, 99.99%) were loaded into quartz ampoules. The ampoules were evacuated to 7.5×10^{-5} Pa, sealed, slowly heated up to 1253 K over 12 h, then kept for 24 h, followed by water quench. The obtained ingots were annealed at 973 K for 7 days. The annealed ingots were ground into powder using an agate mortar, then loaded into a graphite mold with 13 mm diameter and sintered by SPS (SPS-625, Fuji Tec.) under 50 MPa pressure at 873 K for 5 min. The cylinders (Fig. 1d) were cut into bar- and coin-shaped samples (Fig. 1c) in different directions for electrical and thermal transport measurements.

The phase composition was analyzed by powder x-ray diffraction (XRD) analysis using an x-ray diffractometer (Cu K_α radiation, λ = 0.154 nm; Bruker, Germany). The temperature dependence of the electrical conductivity and Seebeck coefficient was tested using an LSR-3 (Linseis) under static helium atmosphere. The thermal conductivity was calculated from the following equation: $\kappa = \rho C_p \lambda$. The temperature dependence of the thermal diffusivity λ was tested by the laser flash method (model LFA-457, Netzsch) under flowing argon atmosphere. The density ρ of the bulk samples was measured by the Archimedes method. The heat capacity value C_p was taken from Chen's work,[18] being calculated from the fitting equation given by Pashinkin[20] and Yamaguchi.[21] The Hall coefficient was determined using a Physical Property Measurement System (PPMS-14, Quantum Design) under magnetic field of −1 T to 1 T. Thermal analysis was carried out using a differential scanning calorimeter (DSC404-F3). The relative density of all samples was over 97% of the theoretical value (6.18 g/cm^3). The Hall mobility was calculated from the relationship $\mu_H = \sigma/ne$, where σ is the electrical conductivity, n is the carrier concentration, and e is the electron charge.

RESULTS

Figure 1a shows the XRD patterns of $Ag_xSn_{1-x}Se$ (x = 0, 0.0025, 0.005, 0.0075, 0.01, 0.02) powders ground from quenched ingots. The patterns can be indexed to the orthorhombic SnSe phase (PDF#48-1224). With increasing Ag content, a small amount of impurity phase gradually emerges in the XRD pattern, indicated by green arrows. The impurity phase was identified as $AgSnSe_2$ phase (PDF#33-1149), consistent with Chen's work.[18] The solubility of Ag in SnSe is very low, being limited to 0.5% or less. The effects of Ag doping and the secondary phase on the lattice parameter are inconspicuous as a result of the minimal doping content. The XRD patterns of the $Ag_xSn_{1-x}Se$ samples were refined using the Rietveld full file fitting method, and the lattice parameter (a = 11.5147 Å, b = 4.159 Å, c = 4.451 Å) was calculated by using the general structure analysis system (GSAS), being consistent with literature.[15]

Figure 1b shows the XRD patterns of the sintered SnSe bulks both perpendicular and parallel to the pressing direction. The XRD patterns parallel to the pressing direction exhibit some preferred orientation. The strongest peak observed is the (400) peak instead of the (111) peak, which is the strongest peak in the standard pattern (PDF#48-1224). Meanwhile, perpendicular to the pressing direction (Fig. 1c, red plane), there is scarcely any preferred orientation in the XRD patterns, and the strongest peak of the bulk samples matches well with the standard pattern, i.e., (111), consistent with prior studies on SnSe.[16,17,22]

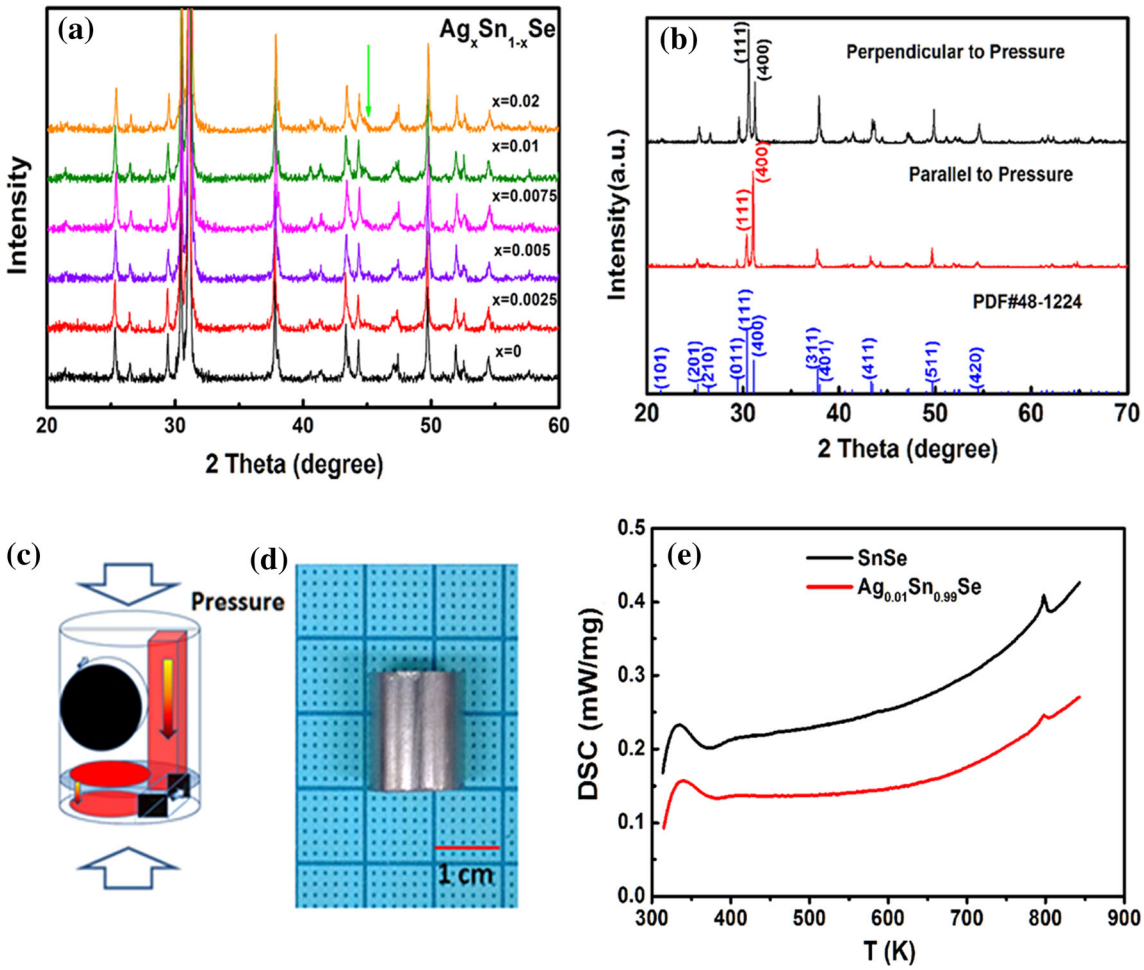

Fig. 1. (a) XRD patterns of $Ag_xSn_{1-x}Se$ (x = 0, 0.0025, 0.005, 0.0075, 0.01, 0.02) powders ground from quenched ingots. (b) XRD patterns of SnSe bulks sintered by SPS both parallel and perpendicular to the pressing direction. (c) Sample cutting direction for measurements parallel and perpendicular to the pressing direction. (d) Bulk sample sintered by SPS. (e) Differential scanning calorimetry (DSC) scans for SnSe and $Ag_{0.01}Sn_{0.99}Se$. Exothermal peaks were observed at 803 K (Color figure online).

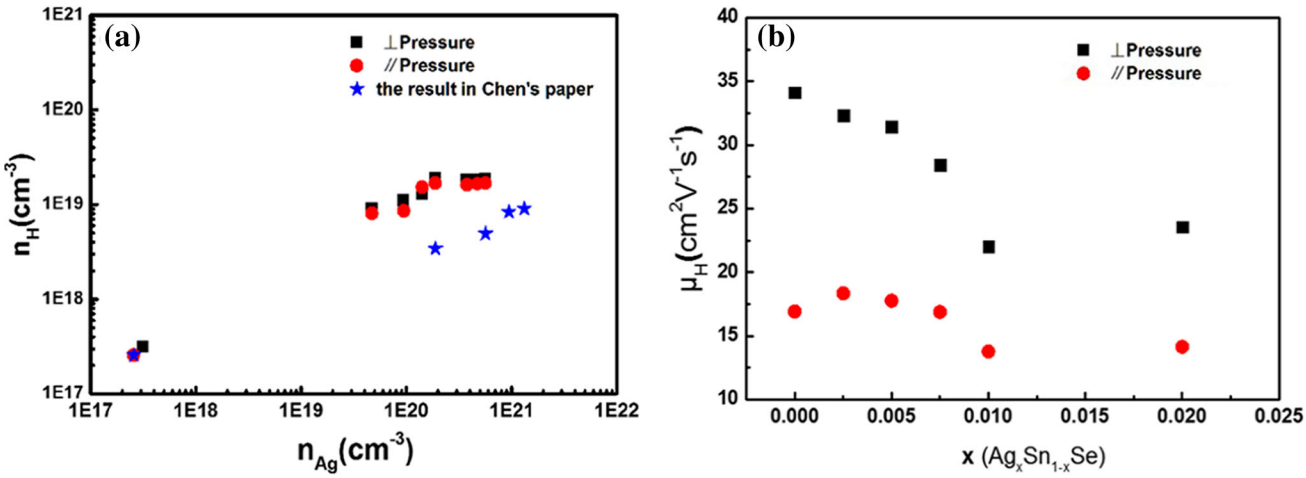

Fig. 2. (a) Measured Hall carrier concentration in the present work and Chen's work[18] as a function of Ag concentration at 300 K. (b) Calculated Hall mobility in the present work as a function of Ag content (x) at 300 K.

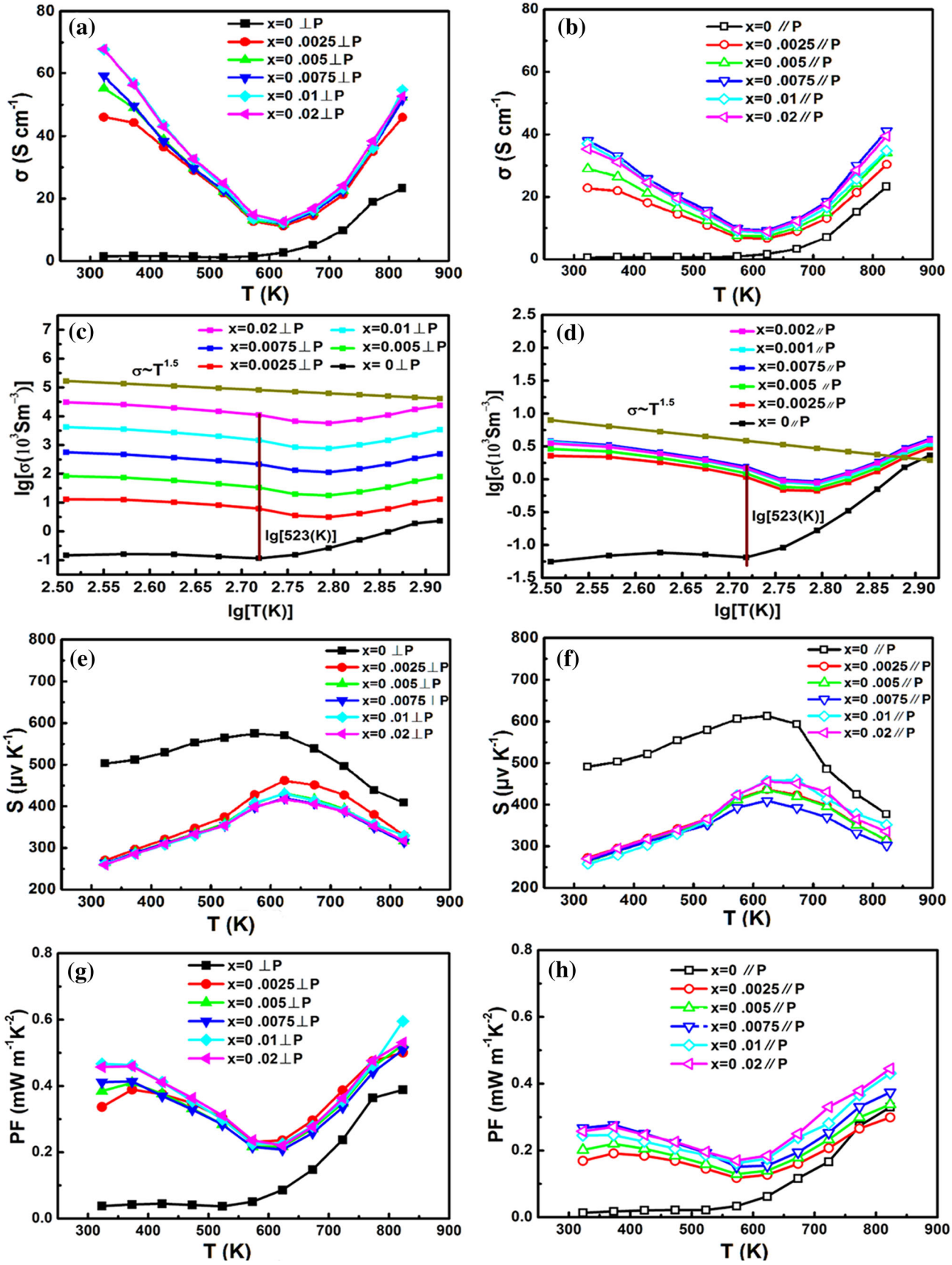
(a)
x=0 ⊥P
x=0 .0025⊥P
x=0 .005⊥P
x=0 .0075⊥P
x=0 .01⊥P
x=0 .02⊥P
σ (S cm-1)
T (K)
(b)
x=0 //P
x=0 .0025//P
x=0 .005//P
x=0 .0075//P
x=0 .01//P
x=0 .02//P
σ (S cm-1)
T (K)
(c)
x=0.02⊥P
x=0.01⊥P
x=0.0075⊥P
x=0.005⊥P
x=0.0025⊥P
x= 0⊥P
σ~T1.5
lg[523(K)]
lg[σ(10³Sm⁻³)]
lg[T(K)]
(d)
x=0.002//P
x=0.001//P
x=0.0075//P
x=0.005 //P
x=0.0025//P
x= 0//P
σ~T1.5
lg[523(K)]
lg[σ(10³Sm⁻³)]
lg[T(K)]
(e)
x=0 ⊥P
x=0 .0025⊥P
x=0 .005⊥P
x=0 .0075⊥P
x=0 .01⊥P
x=0 .02⊥P
S (μv K-1)
T (K)
(f)
x=0 //P
x=0 .0025//P
x=0 .005//P
x=0 .0075//P
x=0 .01//P
x=0 .02//P
S (μv K-1)
T (K)
(g)
x=0 ⊥P
x=0 .0025⊥P
x=0 .005⊥P
x=0 .0075⊥P
x=0 .01⊥P
x=0 .02⊥P
PF (mW m-1K-2)
T (K)
(h)
x=0 //P
x=0 .0025//P
x=0 .005//P
x=0 .0075//P
x=0 .01//P
x=0 .02//P
PF (mW m-1K-2)
T (K)

◀Fig. 3. Electrical conductivity measured (a) perpendicular and (b) parallel to the pressing direction. Logarithmic electrical conductivity (c) perpendicular and (d) parallel to the pressing direction. Seebeck coefficient measured (e) perpendicular and (f) parallel to the pressing direction. Power factor measured (g) perpendicular and (h) parallel to the pressing direction (Color figure online).

Figure 1e shows the DSC results for the sintered SnSe and $Ag_{0.01}Sn_{0.99}Se$ samples. Endothermal peaks are observed in the two curves at 803 K, corresponding to the phase transition from *Pnma* (D_{2h}^{16}) phase to *Cmcm* (D_{2h}^{17}) phase of SnSe. The critical temperature (803 K) of the phase transition is in line with related literature.[23,24]

Figure 2a and b show the Hall carrier concentration and Hall mobility of the $Ag_xSn_{1-x}Se$ samples (x = 0, 0.0025, 0.005, 0.0075, 0.01, 0.02), respectively. The Hall carrier concentration ($\rho_H = R_H e^{-1}$) of undoped SnSe is around 3×10^{17} cm^{-3} at 300 K, roughly of the same level as Chen's report (2.5×10^{17} cm^{-3}).[18] A saturated carrier concentration of 1.9×10^{19} cm^{-3} is obtained for $Ag_{0.01}Sn_{0.99}Se$, which is 52.63% higher than that reported by Chen et al. (9×10^{18} cm^{-3}).[18] With Ag doping, the Hall mobility demonstrates a decreasing trend, because Ag doping induces an increase of both carrier scattering and the point defect concentration. The carrier mobility saturates when the Ag content reaches 0.1, suggesting extremely low solubility of Ag in SnSe. Anisotropy is observed in the Hall carrier mobility. The Hall mobility perpendicular to the pressing direction is always greater than that parallel to the pressing direction, due to the higher carrier mobility in the a-axis corresponding to the direction perpendicular to the pressing direction.[16]

Figure 3a and b shows the temperature dependence of the electrical conductivity for the $Ag_xSn_{1-x}Se$ samples (x = 0, 0.0025, 0.005, 0.0075, 0.01, 0.02). In SnSe, the electrical conductivity is around 1.50 S cm^{-1} at room temperature and increases rapidly to 23.25 S cm^{-1} at 823 K (Fig. 3a and b), indicating typical semiconducting behavior. For the samples with Ag doping, the electrical conductivity displays metallic transport behavior below 623 K, then increases rapidly, suggesting semiconducting behavior caused by thermal excitation of intrinsic semiconducting carriers. A maximum electrical conductivity of 54.78 S cm^{-1} is obtained for $Ag_{0.01}Sn_{0.99}Se$ perpendicular to the pressing direction at room temperature. The electrical conductivity parallel to the pressing direction exhibits lower values than those perpendicular to the pressing direction. This results from the preferred orientation parallel to the pressing direction, which leads to lower carrier mobility parallel to the pressing direction than in other measuring directions.

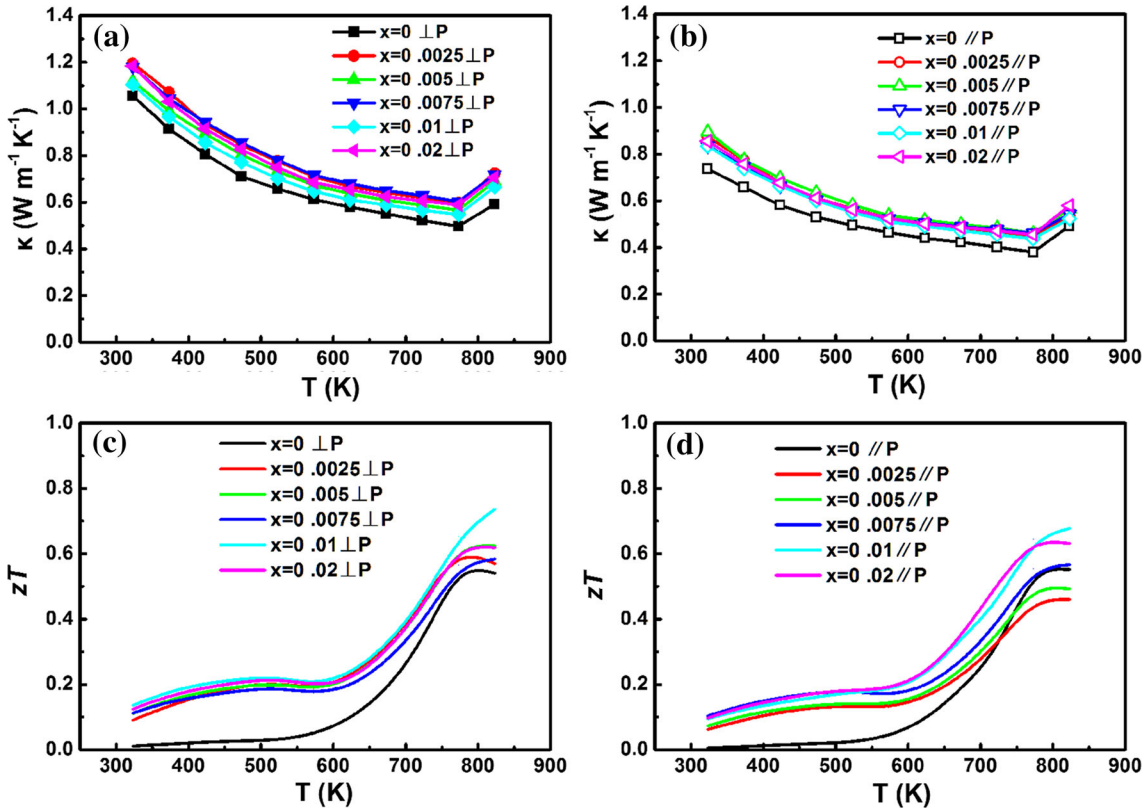

Fig. 4. Thermal conductivity measured (a) perpendicular and (b) parallel to the pressing direction. zT value (c) perpendicular and (d) parallel to the pressing direction (Color figure online).

Figure 3e and f shows the temperature dependence of the Seebeck coefficient for $Ag_xSn_{1-x}Se$ samples (x = 0, 0.0025, 0.005, 0.0075, 0.01, 0.02). In SnSe samples, the Seebeck coefficient is around 500 $\mu V\ K^{-1}$ at room temperature and increases rapidly to 613 $\mu V\ K^{-1}$ at 623 K. Then, the Seebeck coefficient starts to decrease when the temperature is over 623 K. In Ag-doped samples, the trends of the Seebeck coefficient variation also show similar behavior with increasing temperature. The Seebeck coefficient starts to decrease above 623 K due to thermal excitation. Compared with undoped SnSe, the greater drop of the Seebeck coefficient in the Ag-doped SnSe samples results from the increased carrier concentration. Different from the electrical conductivity, the Seebeck coefficient shows scarcely any difference in the two directions.

Figure 3g and h shows the temperature dependence of the power factor (PF) for $Ag_xSn_{1-x}Se$ samples (x = 0, 0.0025, 0.005, 0.0075, 0.01, 0.02) both perpendicular and parallel to the pressing direction. The PF of all the samples was calculated from the measured electrical conductivity and Seebeck coefficient ($PF = S^2\sigma$). A maximum PF of 0.6 $mW\ m^{-1}\ K^{-2}$ was obtained for $Ag_{0.01}Sn_{0.99}Se$ perpendicular to the pressing direction.

Figure 4a and b shows the temperature dependence of the thermal conductivity for $Ag_xSn_{1-x}Se$ samples (x = 0, 0.0025, 0.005, 0.0075, 0.01, 0.02) both perpendicular and parallel to the pressing direction. All the thermal conductivity values remain at a very low level between 0.4 W/m-K and 1.2 W/m-K in the measured temperature range. With increasing temperature, the thermal conductivity decreases due to increased phonon scattering. When the temperature reaches 773 K, the thermal conductivity starts to increase, which is related to the phase transition from Pnma to Cmcm. A minimum thermal conductivity of 0.55 W/m-K was obtained for undoped SnSe at 773 K.

Similar to the electrical conductivity, the thermal conductivity exhibits outstanding anisotropy. The thermal conductivity perpendicular to the pressing direction always exhibits higher values than those parallel to the pressing direction. A minimum thermal conductivity of 0.4 W/m-K was obtained for $Ag_{0.01}Sn_{0.99}Se$ parallel to the pressing direction.

Figure 4c and d shows the temperature dependence of the zT value for $Ag_xSn_{1-x}Se$ samples (x = 0, 0.0025, 0.005, 0.0075, 0.01, 0.02) perpendicular and parallel to the pressing direction, respectively. The zT value of undoped SnSe increases with temperature but starts to decrease above 773 K. A maximum zT value of 0.56 was obtained at 773 K, which is higher than the results reported by Sassi (0.5)[17] and Chen (0.3).[18] For the Ag-doped SnSe, the zT values perpendicular to the pressing direction were higher than those parallel to the pressing direction. A maximum zT value of 0.74 was observed for $Ag_{0.01}Sn_{0.99}Se$ perpendicular to the pressing direction at 823 K.

DISCUSSION

The degree of orientation of the (h00) bc-planes is evaluated by the orientation factor termed F. The orientation factor was calculated by the Lotgering method using the following equations:[25]

$$F = \frac{P - P_0}{1 - P_0}, \tag{1}$$

$$P_0 = \frac{I_0(h00)}{\Sigma I_0(hkl)}, \tag{2}$$

$$P = \frac{I(h00)}{\Sigma I(hkl)}, \tag{3}$$

where P and P_0 are the ratios of the integrated intensities of all (h00) planes to those of all (hkl) planes for preferentially and randomly oriented samples, respectively. In the sintered samples, a high orientation factor of 0.32 was obtained parallel to the pressing direction, which is higher than that (F = 0) perpendicular to the pressing direction. On the one hand, grains cleave easily from the cleavage plane due to the weak, van der Waals bonding between layers and tend to be rearranged under an applied pressure. The basal bc-plane tends to become perpendicular to the pressing direction in this rearrangement process. A series of plate-like polycrystalline $Ag_xSn_{1-x}Se$ structures are stacked along the sintering pressing direction, producing a strong peak in the XRD patterns from (h00) planes, namely a high degree of orientation parallel to the pressing direction. On the other hand, highly oriented texture is related to fine grain size. In general, highly oriented texture is easily obtained when the grain size is large enough,[26] but it becomes difficult to form when the grain size is small.[23] The grain sizes of the polycrystalline SnSe were around 15 μm, contributing to the high degree of orientation. Moreover, we also note that these high F values may be related to the direct-current pulsing during the SPS process.

The significant increase of the electrical conductivity for Ag-doped SnSe is mainly related to the improvement of the carrier concentration in spite of the drop of the Hall carrier mobility. With Ag doping, the carrier concentration increases from $3 \times 10^{17}\ cm^{-3}$ to $1.9 \times 10^{19}\ cm^{-3}$. At the same temperature, the electrical conductivity parallel to the pressing direction is always lower than that in another measuring direction, as a result of the anisotropy in the Hall carrier mobility shown in Fig. 2b. The outstanding anisotropy in the Hall carrier mobility mainly results from the anisotropy of the effective mass. The shape of the Fermi surface indicates that the effective mass possesses its highest value along the a-axis direction (perpendicular to the SnSe layers), corresponding to higher effective mass parallel to the pressing direction.[27] High effective band mass results in low carrier mobility, because the mobility ($\mu = {}^{\tau e}/_{m_I^*}$) is in-

versely proportional to the inertial mass when the carriers are predominantly scattered by phonons. Simultaneously, the scattering time τ decreases with m_b^* and the overall density of states (DOS) effective mass ($m_d^* = N_V^{2/3} m_b^*$) is proportional to the effective band mass when the carriers are predominantly scattered by phonons.[28]

For further discussion, the logarithmic electrical conductivity (LEC) of SnSe-based alloys was calculated and is plotted in Fig. 3c and d. Below 523 K, the LEC of the SnSe-based alloys roughly follows a $T^{-1.5}$ dependence, indicating acoustic phonon scattering. When the temperature is higher than 523 K, the dominant factor in the electrical conductivity undergoes a transition from phonon scattering to thermal excitation of intrinsic carriers. At the beginning of this transition, the LEC of SnSe alloys doped with Ag decreases more rapidly than that of SnSe alloy due to bipolar effects. Above 723 K, the LEC of the SnSe-based alloys roughly follows the dependence of undoped SnSe, suggesting that the dominant effect in the electrical conductivity is the gradual increase in carrier concentration caused by thermal excitation of intrinsic carriers (both holes and electrons).

Corresponding to the rapid increase in the electric conductivity due to bipolar conduction, the Seebeck coefficient shows a rapid decrease above 623 K for the same reason. At low temperatures ($T < 523$ K), the Seebeck coefficient of Ag-doped SnSe shows little change with increase of the Ag content due to the limited increase in the carrier concentration. However, when the temperature is higher than 523 K, the difference in the Seebeck coefficient of Ag-doped SnSe gradually increased. This greater difference at high temperature should be due to suppression of bipolar conduction for the samples with high carrier concentration.

The thermal conductivity showed little change on substitution of Sn with Ag at Sn site, due to the large contribution of phonon conduction to the total thermal conductivity. The decline of the thermal conductivity was slowed by bipolar effects when the temperature was higher than 523 K. Bipolar effects on the thermal conductivity occur when electron–hole pairs absorb heat in a high-temperature region and give out heat by recombining in a low-temperature region within the intrinsic conduction region.[29] However, a difference in the bipolar thermal conductivity between undoped and doped SnSe caused by the remarkable improvement in the carrier concentration is not demonstrated. This can be attributed to the decrease of the bandgap for the Ag-doped SnSe. For a single parabolic band and acoustic phonon scattering ($\lambda = -1/2$), the bipolar thermal conductivity in semiconductors can be expressed as[30]

$$\frac{\left(\frac{k_B}{e}\right)^2\left[\frac{E_g}{k_B T}+\frac{2F_1(\xi_p)}{F_0(\xi_p)}+\frac{2F_1(\xi_n)}{F_0(\xi_n)}\right]^2 T}{\kappa_b}=\frac{1}{\sigma_n}+\frac{1}{\sigma_p}, \quad (4)$$

where k_B is the Boltzmann constant, e is the free electron charge, ξ is the reduced Fermi energy, and F_x is the Fermi integral of order x. Therefore, $\xi_n + \xi_p = -E_g/k_B T$, where E_g is the bandgap. With Ag doping, the bandgap of $Ag_xSn_{1-x}Se$ shows a decreasing trend (as shown in the Electronic Supplementary Material), which weakens the effect on the bipolar thermal conductivity of the increased carrier concentration. The thermal conductivity transition at 773 K is caused by both bipolar thermal conductivity and the phase transition from low-temperature *Pnma* phase to *Cmcm* phase. Compared with the *Cmcm* phase, the thermal conductivity of the *Pnma* phase is lower, which is ascribed to strong bonding anharmonicity. The *Pnma* phase with zigzag geometrical structure can be deformed like a retractable spring in the (l00) plane, which is called a soft lattice. Moreover, the elastic net formed due to the weaker bonding between SnSe slabs also restricts phonon transport. All the above-mentioned effects can give rise to low lattice thermal conductivity in ordered crystal structures.[31–33]

CONCLUSIONS

Polycrystalline Ag-doped SnSe compounds were prepared by melting and SPS methods. Ag is an effective dopant in SnSe compounds. The carrier concentration was immensely enhanced from 3×10^{17} cm^{-3} to 1.9×10^{19} cm^{-3} for $Ag_{0.01}Sn_{0.99}Se$ at room temperature. All the $Ag_xSn_{1-x}Se$ compounds showed anisotropic thermoelectric properties. Perpendicular to the pressing direction, a maximum zT value of 0.74 was obtained for $Ag_{0.01}Sn_{0.99}Se$ at 823 K, being 23% higher than that of SnSe compounds ($zT = 0.6$). Parallel to the pressing direction, a maximum zT value of 0.68 was obtained for $Ag_{0.01}Sn_{0.99}Se$ at 823 K.

ELECTRONIC SUPPLEMENTARY MATERIAL

The online version of this article (doi: 10.1007/s11664-015-4143-4) contains supplementary material, which is available to authorized users.

REFERENCES

1. G.S. Nolas, J. Sharp, and J. Goldsmid, *Thermoelectrics: basic principles and new materials developments*, Vol. 45 (New York: Springer-Verlag Berlin Heidelberg, 2001).
2. D.R. Brown, T. Day, K.A. Borup, S. Christensen, B.B. Iversen, and G.J. Snyder, *APL Mater.* 1, 052107 (2013).
3. H. Zhu, W.H. Sun, R. Armiento, P. Lazic, and G. Ceder, *Appl. Phys. Lett.* 104, 082107 (2014).
4. X.G. Wang, L. Wang, J. Liu, and L.M. Peng, *Appl. Phys. Lett.* 104, 132106 (2014).
5. Q. Zhang, X. Ai, W. Wang, L. Wang, and W. Jiang, *Acta Mater.* 73, 37 (2014).

6. Q. Zhang, X. Ai, L. Wang, Y. Chang, W. Luo, W. Jiang, and L. Chen, *Adv. Funct. Mater.* 25, 966 (2015).
7. M. Zhou, J.-F. Li, H. Wang, T. Kita, L. Li, and Z. Chen, *J. Electron. Mater.* 40, 862 (2011).
8. W.J. Xie, X.F. Tang, Y.G. Yan, Q.J. Zhang, and T.M. Tritt, *Appl. Phys. Lett.* 94, 102111 (2009).
9. A.D. LaLonde, Y. Pei, H. Wang, and G.J. Snyder. *Mater. Today* 14, 526 (2011).
10. J.P. Heremans, V. Jovovic, E.S. Toberer, A. Saramat, K. Kurosaki, A. Charoenphakdee, S. Yamanaka, and G.J. Snyder, *Science* 321, 554 (2008).
11. H. Wang, Y. Pei, A.D. LaLonde, and G.J. Snyder, *Adv. Mater.* 23, 1366 (2011).
12. T.H. Zou, X.Y. Qin, D. Li, G.L. Sun, Y.C. Dou, Q.Q. Wang, B.J. Ren, J. Zhang, H.X. Xin, and Y.Y. Li, *Appl. Phys. Lett.* 104, 013904 (2014).
13. S.A. McDonald, G. Konstantatos, S. Zhang, P.W. Cyr, E.J.D. Klem, L. Levina, and E.H. Sargent, *Nat. Mater.* 4, 138 (2005).
14. L.D. Zhao, S.H. Lo, J. He, H. Li, K. Biswas, J. Androulakis, C.I. Wu, T.P. Hogan, D.-Y. Chung, V.P. Dravid, and M.G. Kanatzidis, *J. Am. Chem. Soc.* 133, 20476 (2011).
15. C. Guillén, J. Montero, and J. Herrero, *Phys. Status Solidi (a)* 208, 679 (2011).
16. L.D. Zhao, S.H. Lo, Y. Zhang, H. Sun, G. Tan, C. Uher, C. Wolverton, V.P. Dravid, and M.G. Kanatzidis, *Nature* 508, 373 (2014).
17. S. Sassi, C. Candolfi, J.B. Vaney, V. Ohorodniichuk, P. Masschelein, A. Dauscher, and B. Lenoir, *Appl. Phys. Lett.* 104, 212105 (2014).
18. C.-L. Chen, H. Wang, Y.-Y. Chen, T. Day, and G.J. Snyder, *J. Mater. Chem. A* 2, 11171 (2014).
19. A. Bellosi, F. Monteverde, and D. Sciti, *Int. J. Appl. Ceram. Technol.* 3, 32 (2006).
20. A.S. Pashinkin, A.S. Malkova, V.A. Fedorov, and M.S. Mikhailova, *Inorg. Mater.* 42, 593 (2006).
21. K. Yamaguchi, K. Kameda, Y. Takeda, and K. Itagaki, *Mater. Trans. JIM* 35, 118 (1994).
22. S. Chen, K. Cai, and W. Zhao, *Phys. B Condens. Matter* 407, 4154 (2012).
23. H.I.K. Fukuda, T. Ishii, F. Toyoda, M. Yamanashi, and Y. Kibayashi, *Fifteenth International Conference on IEEE*, vol. 37, 1996.
24. William J. Baumgardner, Joshua J. Choi, Yee-Fun Lim, and Tobias Hanrath, *J. Am. Chem. Soc.* 132, 9519 (2010).
25. F. Lotgering, *J. Inorg. Nucl. Chem.* 9, 113 (1959).
26. J. Jiang, L. Chen, S. Bai, Q. Yao, and Q. Wang, *Mater. Sci. Eng. B* 117, 334 (2005).
27. K. Kutorasinski, B. Wiendlocha, S. Kaprzyk, and J. Tobola, *Phys. Rev. B* 91, 205201 (2015).
28. Y. Pei, H. Wang, and G.J. Snyder, *Adv. Mater.* 24, 6125 (2012).
29. H. Julian Goldsmid *Introduction to Thermoelectricity*, Vol. 34 (New York: Springer-Verlag Berlin Heidelberg, 2001).
30. S. Wang, J. Yang, T. Toll, J. Yang, W. Zhang, and X. Tang, *Sci. Rep.* 5, 10136 (2015).
31. D. Morelli, V. Jovovic, and J. Heremans, *Phys. Rev. Lett.* 101, 035901 (2008).
32. M.D. Nielsen, V. Ozolins, and J.P. Heremans, *Energy Environ. Sci.* 6, 570 (2013).
33. Y. Zhang, E. Skoug, J. Cain, V. Ozolinš, D. Morelli, and C. Wolverton, *Phys. Rev. B* 85, 054306 (2012).